Increasing salinity of fibrinogen solvent generates stable fibrin hydrogels for cell delivery or tissue engineering

Dillon K. Jarrell[1], Ethan J. Vanderslice[1], Mallory L. Lennon[1], Anne C. Lyons[1], Mitchell C. VeDepo, PhD[1], Jeffrey G. Jacot, PhD[1,2,*]

[1] Department of Bioengineering, University of Colorado Anschutz Medical Campus, Aurora, CO, USA 80045

[2] Department of Pediatrics, Children's Hospital Colorado, Aurora, CO, USA 80045

* Corresponding author

Email: jeffreyjacot@cuanschutz.edu

ORCID: https://orcid.org/0000-0002-1272-5055

Abstract

Fibrin has been used clinically for wound coverings, surgical glues, and cell delivery because of its affordability, cytocompatibility, and ability to modulate angiogenesis and inflammation. However, its rapid degradation rate has limited its usefulness as a scaffold for 3D cell culture and tissue engineering. Previous studies have sought to slow the degradation rate of fibrin with the addition of proteolysis inhibitors or synthetic crosslinkers that require multiple functionalization or polymerization steps. These strategies are difficult to implement *in vivo* and introduce increased complexity, both of which hinder the use of fibrin in research and medicine. Previously, we demonstrated that the simple inclusion of bifunctionalized poly(ethylene glycol)-n-hydroxysuccinimide (PEG-NHS) in the fibrinogen solvent slows the degradation rate of fibrin by providing additional crosslinking. In this study, we aimed to further improve the longevity of fibrin gels such that they could be used for tissue engineering in vitro or in situ without the need for proteolysis inhibitors. It is well documented that increasing the salinity of fibrin precursor solutions affects the resulting gel morphology. In this study, we investigated whether this altered morphology influences the fibrin degradation rate. Increasing the final sodium chloride (NaCl) concentration from 145 mM (physiologic level) to 250 mM resulted in fine, transparent high-salt (HS) fibrin gels that degrade 2-3 times slower than coarse, opaque physiologic-salt (PS) fibrin gels both *in vitro* (when treated with proteases and when seeded with amniotic fluid stem cells) and *in vivo* (when injected subcutaneously into mice). Increased salt concentrations did not affect the viability of encapsulated cells, the ability of encapsulated endothelial cells to form rudimentary capillary networks, or the ability of the gels to maintain induced pluripotent stem cells. Finally, when implanted subcutaneously, PS gels degraded completely within one week while HS gels remained stable and maintained viability of seeded dermal fibroblasts. To our knowledge, this is the simplest method reported for the fabrication of fibrin gels with tunable degradation properties and will be useful for implementing fibrin gels in a wide range of research and clinical applications.

1. Introduction

The development of thick tissues for the repair of large injuries or defects is a principal challenge for tissue engineering advancements (1-4). *In vitro* tissue engineering approaches face the challenges of nutrient diffusion and recapitulation of tissue-specific signaling outside of the body while *in situ* tissue engineering approaches must promote normal tissue regeneration while avoiding fibrosis and aberrant tissue growth (5). Both strategies

must include scaffolds that support the proliferation and differentiation of tissue-specific stem cells while simultaneously degrading and being replaced with tissue-specific extracellular matrix (6, 7).

Natural hydrogels make promising tissue engineering scaffolds because they are cytocompatible, bioactive, and readily remodeled by cells. The bioactivity of fibrin is particularly attractive since fibrin clots drive wound healing in the body by modulating inflammation, angiogenesis, and cell-matrix interactions (8-11). Not surprisingly, fibrin glues and gels have been extensively investigated for use in wound sealing and the delivery of growth factors and cells. Despite this desirable bioactivity, the rapid degradation rate of fibrin has limited its usefulness as a scaffold for 3D cell culture and tissue engineering. Plasmin inhibitors such as 6-aminocaproic acid (ACA) prevent fibrinolysis but are difficult to implement *in vivo* (12). Therefore, we aimed to develop a slowly-degrading ("stable") fibrin gel capable of supporting 1) the proliferation and differentiation of various stem cell types, 2) the development of a rudimentary capillary-like network *in vitro*, and 3) delivery and maintenance of cells *in vivo* without the need for degradation inhibitors.

Our group is interested in engineering tissues by differentiating amniotic fluid cells (AFC) or induced pluripotent stem cells (iPSC) in 3D. Most differentiation protocols for these two stem cell types require at least two weeks of culture, so a suitable fibrin scaffold must be stable when seeded with these cell types for at least two weeks. We previously reported that increased gel crosslinking using homobifunctional poly(ethylene glycol) n-hydroxysuccinimide (PEG-NHS) slows fibrin degradation when placed in media alone (13, 14), but our follow-up work reported here demonstrates that even these PEG-fibrin gels degrade within one week when seeded with AFC (note that the PEG-fibrin gels reported in our previous studies are identical to the PS gels reported here). To further reduce the rate of fibrin degradation, we sought to manipulate other fibrin composition variables. It is known that several properties of fibrin, including opacity, morphology, and mechanics, can be controlled by several composition variables, including pH, salinity, buffer type, crosslinkers, and the concentrations of fibrinogen, thrombin, and calcium (15-21). Ferry et al. first reported that "fine" (transparent) and "coarse" (opaque) fibrin clots could be generated by adjusting pH and ionicity (22, 23); Eyrich and colleagues expanded on this work by demonstrating that only fine, transparent fibrin can maintain 3D chondrocyte culture without degrading (24). A similar study by Davis and colleagues found that increasing sodium chloride in the gel precursor improved the gel mechanical properties and osteogenic behavior of seeded mesenchymal stem cells (25). These results can likely be explained by the effects of chlorine ions on fibrin polymerization, as chlorine is

known to bind fibrin and oppose lateral aggregation of protofibrils, resulting in thin, dense networks (26, 27). Another group decreased the rate of fibrinolysis by fusing an engineered peptide sequence derived from alpha-2 plasmin inhibitor to recombinant VEGF and covalently linking it to fibrin during gelation (28). This strategy proved exceedingly effective, but is complicated, expensive, time consuming, and requires specific laboratory expertise. Robinson and colleagues also effectively decreased fibrinolysis using genipin crosslinking, which also exhibits neuritogenic effects (29). While these effects were beneficial in their elegant formulation, they would be detrimental in most systems.

In this study, we found that increasing the salinity (NaCl concentration) of the fibrinogen precursor solution generates increasingly transparent fibrin with decreasing rates of degradation. We investigated the ability of these gels to support encapsulated induced pluripotent stem cells (iPSC) and amniotic fluid cells (AFC) *in vitro*. We also assessed the ability of the gels to support vascularization both *in vitro* and *in vivo*. Increased salinity during gelation did not affect the viability of encapsulated cells and the high-salt (HS) gels supported encapsulated AFC without degrading for at least two weeks. Both the physiologic-salt (PS) and HS gel formulations were able to maintain iPSC and support capillary-like network formation *in vitro* when seeded with human endothelial cells and fibroblasts. Finally, we found that HS fibrin gels are stable and maintain the viability of seeded cells when implanted subcutaneously into mice, while PS gels degraded completely within one week.

2. Materials and Methods

2.1. Fibrin Gel Fabrication

Fibrin gels were fabricated in four steps**.** First, sterile fibrinogen from human plasma (Millipore Sigma, 341576) was dissolved in sterile PBS (Corning, 21-040-CM) at 80 mg/mL at 37C for two hours. Second, PEG-NHS (3.4 kDa, SUNBRIGHT DE-034HS, NOF America Corporation) was dissolved in PBS at 8 mg/mL, syringe filtered, and immediately mixed with the dissolved fibrinogen 1:1 by volume (PEG:fibrinogen mole ratio of 10:1). The fibrinogen and PEG were allowed to crosslink for one hour at 37C. Third, cells were dissociated with Accutase®, counted, and resuspended in growth media at 4X the desired final cell concentration. The 4X cell and fibrinogen-PEG solutions were mixed 1:1 by volume (PBS control added for cell-free gels) and the mixture was added to the appropriate culture vessel. Fourth, thrombin from human plasma (Millipore Sigma, 605190) was resuspended in cold calcium chloride solution (11.1 mM $CaCl_2$, 145 mM NaCl, pH 7.4 in DI water) at 20 U/mL. Thrombin

solution was added to the cell-fibrinogen-PEG solution 1:1 by volume and quickly mixed by pipetting five times. Gelation occurred at 37C for 5 minutes before gels were immersed in media or PBS. For cell experiments, media was replenished daily. PS and HS gels were fabricated with final concentrations of 10 mg/mL fibrinogen, 1 mg/mL PEG, 1 U/mL thrombin, 5 mM $CaCl_2$, and pH 7.4. PS fibrin was fabricated with a final NaCl concentration of 145 mM (physiologic concentration), and HS fibrin was fabricated with a final NaCl concentration of 250 mM. NaCl concentration was adjusted by adding NaCl to the PBS used as the solvent for the fibrinogen and PEG.

2.2. Measuring Fibrin Opacity

To assess which formulation variables are necessary to generate fine transparent fibrin, 50 uL gels were fabricated in the wells of a 96-well plate. Fibrin opacity was quantified by absorbance spectrophotometry at 352 nm (BioTek Synergy 2, Gen5 software). The gel formulation variables included final fibrinogen concentration (2.5, 5, 10, and 20 mg/mL), gel pH (6, 7, 7.4, 8, 8.5), final $CaCl_2$ concentration (0.1, 0.5, 5, 10, 25 mM), and final NaCl concentration (145, 175, 200, 250, 300 mM). These parameters were investigated independently; the constant gel formulation values were 10 mg/mL fibrinogen, pH 7.4, 5 mM $CaCl_2$, and 145 mM NaCl. Gel pH was adjusted by changing the pH in the $CaCl_2$ solution via 0.1 M NaOH. Salinity was adjusting by changing the NaCl concentrations in the PBS used for the fibrinogen and PEG solutions. The PEG:fibrinogen mole ratio remained 10:1 for all fibrinogen concentrations.

2.3. Scanning electron microscopy

Analysis of gel morphology was assessed using 200 uL fibrin gels in a 48-well tissue culture plate (Corning). After gelation, gels were hydrated in PBS for one hour, then dehydrated in ethanol (50%, 75%, 90%, and 100% ethanol for one hour each). Samples were attached to SEM stubs using double-sided carbon tape and coated with Au/Pd for 30 seconds using an EM ACE200 sputtercoater (Leica, Buffalo Grove, IL, USA). Images were collected with a JSM-6010LA SEM (JEOL, Tokyo, Japan). Analysis of fibers and pores in each gel were quantified using DiameterJ (30). Each greyscale SEM image was segmented using the DiameterJ traditional segmentation algorithm to produce eight 8-bit black and white segmentations per SEM image. The best segmentation of the eight was selected based on the following criteria: (1) no partial fiber segmentations, (2) the intersections of fibers do not contain black spots (i.e. holes), (3) segmented fibers are representative of actual fibers in the image and are not background/imaging artifacts, and (4) segmentations accurately represent fibers'

actual diameter. The selected segmentations were scaled and processed in DiameterJ to quantify pore and fiber characteristics.

2.4. Atomic force microscopy

To analyze compressive modulus at a micro scale, 30 uL fibrin gels were fabricated as drops in 35-mm dishes and submerged in PBS. AFM indentation experiments were performed with a NanoWizard 4a (JPK Instruments) using a cantilever with a nominal spring constant of 0.03 N/m and a pyramidal tip (MLCT-D, Bruker AFM Probes). The dishes were maintained at 37°C during force measurements. Force curves were recorded from three separate regions on the surface of each hydrogel. At each region, 36 force curves were measured across a 100um^2 area for a total of 108 measurements per gel. The data was analyzed using JPK image processing software. Young's modulus was calculated using the Hertz model of fit on the extend curve, and data is represented as mean +/- standard deviation.

2.5. Parallel plate rheology

To analyze the bulk Storage and Young's moduli, 160 uL HS and PS fibrin gels were fabricated as drops in 10-cm dishes and submerged in PBS at 37°C overnight. Gels were carefully dislodged from the plate bottom and moduli were measured using a parallel-plate rheometer (Discovery Hybrid 2; TA Instruments) for five replicates of each hydrogel formulation. Samples were subjected to shear at 1% strain through a dynamic angular frequency range of 0.1 to 100 rad/s. Elastic modulus (E) was calculated from storage modulus (G') by assuming a Poisson's ratio of 0.5.

2.6. Swelling ratio

To assess swelling ratio, 50 uL fibrin gels were fabricated at 145, 175, and 250 mM NaCl as drops in a 10 cm tissue culture-treated dish (Corning). After equilibrating in sterile PBS at 37C overnight, the gels were scraped from the plate using a cell scraper and the wet weight was obtained after dabbing off excess PBS.

2.7. Growth factor release

To assess the ability to release growth factors, 50 uL HS (250 mM NaCl) and PS (145 mM NaCl) gels (10 mg/mL fibrinogen) were fabricated with 100 ng/mL FGF-2 (Peprotech, 100-18b) and 100 ng/mL VEGF-165 (Shenandoah Biotechnology, 100-44) in the bottom of 1.6 mL Eppendorf tubes. To fabricate these gels, a PBS

solution of 400 ng/mL FGF-2 and 400 ng/mL VEGF-165 was used instead of the normal 4X cell solution in Step 3 of Section 2.1 above. After gelation, 1 mL of 0.5% protease-free BSA (Sigma, A3059) in PBS was added to each tube and was completely replaced daily. After 0, 1, and 7 days, the supernatant was removed and 50 uL of 0.2 mg/mL human plasmin (Enzyme Research Laboratories) in HEPES buffer (pH 8.5, Boston Bioproducts) was added. Fibrin degradation occurred overnight at 37C. Growth factor retention was measured using ELISAs (Peprotech, 900-K08 and 900-K10) and a BioTek Synergy 2 luminescent plate reader (Gen5 software).

2.8. Papain-mediated degradation

To analyze the fibrin degradation kinetics as a function of salinity, 75 uL fibrin gels were fabricated at 145, 175, and 250 mM NaCl as drops in 10 cm tissue culture-treated dishes and were allowed to equilibrate in PBS at 37C for one hour. At time zero, 10 mL of warm protease solution consisting of 0.8 uM Papain (21 kDa, Sigma, P4762) and 2.7 mM N-acetylcysteine (Sigma, A7250) in PBS was added to each dish. Every 10 minutes for one hour, three gels from each formulation were scraped from the dish, dabbed on a KimWipe, and weighed.

2.9. Cell viability and Cell-mediated degradation

To analyze cell viability in the HS fibrin gels, passage 3-5 AFC were dissociated and resuspended in EGM-2 (Lonza) at $4x10^5$ cells/mL. 75 uL HS (250 mM NaCl) and PS (145 mM NaCl) fibrin gels were fabricated using the 4X AFC suspension as drops in wells of a 6-well tissue culture-treated plate (three gels per well). After gelation, 2 mL of EGM-2 was added to each well and the gels were incubated at 37°C and 5% CO_2. After 1, 24, and 96 hours, EGM-2 was aspirated and cells were stained using the fluorescent LIVE/DEAD Viability/Cytotoxicity Kit (Invitrogen) according to kit instructions. Three images were captured from each gel using a Zeiss Observer.Z1 and long-distance objective (LD Plan-NEOFLUAR 20X/0,4 Ph2) and were used to count living and dead cells.

To analyze the cell-mediated degradation kinetics of HS and PS fibrin formulations, gels were fabricated with a final concentration of $1x10^5$ AFC/mL (P3-5) and incubated in EGM-2 +/- 1 mg/mL of the plasmin inhibitor 6-aminocaproic acid (Sigma, A2504) at 37°C and 5% CO_2. After 0, 7, and 14 days, gels were imaged using phase contrast (Zeiss ObserverZ.1) and wet weights were recorded.

2.10. iPSC encapsulation

iC4-4 iPSC (31) were purchased from the Gates Center for Regenerative Medicine at the University of Colorado. iPSCs were maintained in mTeSR-1 (StemCell Technologies) on 6-well tissue culture plates coated with Matrigel® (Corning). Media was replenished daily, and cells were passaged as colonies every 4-5 days using 0.5 mM EDTA. iPSC (P20-30) were dissociated with Accutase®, centrifuged for 3 minutes at 300 rcf, and resuspended in mTeSR-1 with 10 uM ROCK inhibitor (Y-27632, Sigma**)** at $4x10^6$ cells/mL. 30 uL HS and PS fibrin gels were fabricated using the 4X iPSC suspension as drops in a 6-well plate (three gels per well). After gelation, 2 mL of mTeSR-1 plus 10 uM ROCK inhibitor was added, after which mTeSR-1 alone was replenished daily. After 24 and 96 hours, gels were imaged using phase contrast and analyzed for pluripotency markers using PCR. Briefly, to analyze mRNA expression, whole gels were scraped from the plate and homogenized in TriZol (Life technologies). RNA was extracted in chloroform and washed using the Qiagen RNeasy Minikit. Reverse transcription was conducted using the High-Capacity cDNA Reverse Transcription Kit (Applied Biosystems) according to kit instructions. Pluripotency genes POU5F1 (ThermoFisher, hs04260367_gH) and NANOG (ThermoFisher, hs04260366_g1) were measured, and Ct values were normalized to GAPDH (Thermofisher, hs02758991_g1) and gene expression of monolayer iPSC cultured on Matrigel® at matching timepoints ($2^{\Delta\Delta Ct}$ method).

2.11. Capillary-like network formation *in vitro*

P3-5 GFP-HUVECs (Angio-Proteomie cAP-0001GFP) and P3-5 human dermal fibroblasts (HDFs, Lonza CC-2509) were dissociated, counted, and resuspended in EGM-2 at $3.2E^6$ cells/mL (4:1 HUVEC:HDF ratio). This 4X cell solution was used to fabricate 100 uL HS and PS gels in wells of a 48-well tissue culture plate. After 7 days, gels were analyzed for network formation using immunofluorescence. Briefly, whole gels were fixed in 4% paraformaldehyde for 30 minutes at room temperature, washed, blocked with 3% BSA and 1% FBS in PBS for one hour, and stained with anti-α-smooth muscle actin (Sigma, C6198, 1:200) in blocking solution for two hours. After three 15-minute PBS washes, cells were stained with DAPI and imaged using a Zeiss ObserverZ.1 fluorescent microscope.

2.12. Subcutaneous injection of fibrin gels

In vivo degradation of fibrin gels was assessed through subcutaneous injection of cell-seeded HS and PS gels in athymic nude mice (6-7 weeks old, $Foxn1^{nu}$; Envigo) in a protocol approved by the Institutional Animal Care

and Use Committees at the University of Colorado Anschutz Medical Campus (protocol #00564). Injections were performed as previously described [23]. Briefly, 500-uL HS and PS gels + $5E^5$ cells/mL were fabricated in 1-mL syringes (n = 4 gels per group). The cell suspension contained a 2:1 ratio of GFP-HUVECs (Lonza) and HDFs. Mice were anesthetized with isoflurane and two gels were implanted into opposite dorsal, posterior pockets. After 7 days, mice were sacrificed and fibrin hydrogels were explanted while retaining the surrounding tissue.

2.13. Histology

Tissues were fixed in formalin for 48h and sent to the Biorepository Core Facility at the University of Colorado Anschutz Medical Campus for paraffin embedding, sectioning, and H&E staining. For immunofluorescence analysis, sections first underwent antigen retrieval via incubation in citrate buffer (10 mM citric acid, 0.05% tween, pH 6.0) at 95C for 10 minutes. To analyze cell delivery and morphology, slides were stained with anti-Vimentin (Sigma, C9080, 1:200), and DAPI.

2.14. Statistics

Data is presented as mean +/- standard error of mean, unless otherwise noted. One-way analysis of variance (ANOVA) followed by a *post hoc* bonferroni correction for multiple comparisons was performed for all comparisons. A value of $p < 0.05$ was considered significant in all tests.

3. Results and Discussion

3.1. Fine, transparent fibrin gels can be fabricated by increasing NaCl concentration alone

Motivated by the findings of other groups that fibrin degradation rate is correlated to its opacity (22-24), we generated fibrin gels with varying pH and concentrations of thrombin, fibrinogen, $CaCl_2$, and NaCl and proceeded to measure gel opacity. In contrast to the some of these studies we found that fibrin opacity does not depend on formulation pH or $CaCl_2$ concentration (Figs 1A and 1B) and that fibrin opacity always increases as fibrinogen concentration increases (Fig 1C). Instead, we report the novel finding that simply increasing the concentration of NaCl in the fibrinogen solution yields transparent fibrin gels (Figs 1D and 1E). Since this trend plateaus above a final NaCl concentration of 250 mM (Fig 1D), this formulation (denoted HS fibrin) was selected for the remaining experiments.

Having fabricated transparent fibrin gels, we next sought to analyze differences in gel morphology. SEM imaging confirmed that the turbid, coarse PS gels consist of a loose network of fibrils while the fine HS gels consist of a dense network of thin fibrils (Figs 2A-C), consistent with previous studies (25, 26). Parallel plate rheology revealed that increased NaCl did indeed increase the bulk Storage and Young's moduli of the hydrogels (3.58 kPa for HS gels versus 0.57 kPa for PS gels, Figs 2E and 2F). AFM analysis revealed that the fibrils of the turbid PS gels were exceedingly varied in Young's modulus; values ranged from 0.5 kPa to 158 kPa and were clearly more heterogeneous than HS gels in SEM images (Fig 2D). In contrast, the elastic moduli of the HS fibrils were more homogeneous at all NaCl concentrations greater than 200 mM, perhaps indicating a critical chlorine concentration that is able to alter the polymerization of 10 mg/mL fibrinogen. To investigate this hypothesis, 200 mM gels were chosen for SEM analysis. In addition, HS gels were larger in volume than PS gels of equal fibrinogen content after reaching equilibrium (Fig 2G), implicating altered water-handling due to the differences in fiber morphology.

Finally, since fibrin is known to sequester growth factors through its heparin-binding domain (11), we hypothesized that the increased number of fibrils in HS gels would better sequester the angiogenic growth factors FGF-2 and $VEGF_{165}$. As expected, the HS gels released $VEGF_{165}$ more slowly than the PS gels, however both gel types released FGF-2 at the same rate and reached the same steady-state value of FGF-2 and $VEGF_{165}$ retention after 7 days (Fig 2H).

3.2. Transparent HS fibrin is stable and supports formation of capillary-like networks *in vitro*

Next, we examined how increased salt concentrations and the resulting altered fibrin morphologies influence encapsulated cell viability, gel degradation rate, and capillary-like network formation. Amniotic fluid cells (AFCs) were selected for testing because of their mesenchymal stem cell-like potency and their usefulness in pediatric regenerative medicine (Supp Fig 1) (32, 33). Since cells encapsulated in HS gels are briefly exposed to super-physiologic NaCl concentrations during fabrication, we examined cell viability after encapsulation using a LIVE/DEAD® immunofluorescence assay (Figs 3A-F). Compared to cells in PS gels, we found no difference in AFC viability at early (1h, 24h) or late (96h) timepoints (Fig 3I).

We previously demonstrated that PS gels support capillary-like network formation *in vitro* (13, 14). To confirm that HS fibrin retains this ability, we co-seeded human dermal fibroblasts (HDF) and green fluorescent protein-

labeled human umbilical vein endothelial cells (GFP-HUVEC). After 7 days, whole gels were fixed, stained with anti-α smooth muscle actin (α-SMA) and imaged. HS and PS gels both supported branching and network formation, with clear overlap of GFP-HUVEC and α-SMA-expressing HDF (Figs 3G and 3H).

Finally, PS and HS gel degradation was investigated using a non-specific protease or encapsulated AFCs. When treated with papain (non-specific protease), the degradation rate decreased as salt concentration increased (Fig 4A). PS gels degraded approximately two times faster than HS gels and also more quickly than gels formed with an intermediate salt concentration (175 mM NaCl). This confirmed the observation made by Eyrich et al. that transparent fibrin gels are more stable (24), as well as confirmed our hypothesis that increased ionicity leads to a more stable gel. A similar trend was observed when gels were degraded by encapsulated AFC. By day 7 post-encapsulation, PS gels were significantly degraded while HS gels remained intact (Figs 4B and 4F). After two weeks of culture, PS gels were nearly-completely degraded, leaving a few gel remnants and a monolayer of viable cells on the surface of the plate (Figs 4G-I). In contrast, HS gels retained 80.6 +/- 7.8% of their wet weight and continued to support 3D culture of proliferating AFC (Figs 4B and G-I). In both groups, fibrinolysis was prevented with the addition of 1 mg/mL ACA to EGM-2 (Fig 4B), which confirms that gel degradation is due to plasmin release from seeded cells. Interestingly, while the PS gels degraded significantly after 7 days when seeded with AFC only, the PS gels were stable after 7 days when seeded with HDF and HUVEC (Fig 3H). This is likely because HDF rapidly produce extracellular matrix proteins like collagen, which offset the concurrent degradation of fibrin.

3.3. Transparent HS fibrin is stable *in vivo* and maintains viability of delivered cells

After determining that HS gels are more stable *in vitro* when seeded with AFCs or treated with proteases, we sought to investigate the behavior of the gels *in vivo*. We have previously shown that the inclusion of PEG in our PS fibrin gels improves longevity *in vivo* (13), and we followed the same subcutaneous gel injection protocol to assess differences between HS and PS hydrogel degradation and ability to support delivered cells. Furthermore, we included GFP-HUVEC and HDF to see if the gel(s) could support vascularization and angiogenesis once injected. HS and PS gels were seeded with GFP-HUVEC and HDF, injected subcutaneously into athymic nude mice, and explanted one week later (Fig 5N). Hematoxylin and eosin staining clearly revealed that the HS gels remained stable and intact after one week while the PS gels were completely degraded (Figs 5A, B, H, and I). *In vitro*, the HDFs prevented even PS gel degradation. However, it is likely that the host innate immune system

increased proteolysis *in vivo*, resulting in PS gel degradation despite HDF seeding. Further analysis using anti-Vimentin staining and fluorescent imagining revealed viable HDF throughout the stable HS gels interspersed with GFP-HUVEC, but little to no capillary formation (Figs 5C-G). While α-SMA was used for *in vitro* staining, vimentin was used for the *in vivo* portion of this work because we found that it specifically labeled the delivered HDFs. In contrast, the explanted skin and underlying fat and muscle tissue surrounding the PS gels revealed no surviving HDF, no GFP-HUVEC, and no gel remnants (Figs 5J-M). Initially, we hypothesized that the HS gels would be most useful for large tissue defect applications and that the PS gels would be most useful for rapid cell delivery applications, however this experiment suggests that the HS gels maintain cell viability better than the PS gels and may be superior for both applications.

3.4. HS and PS fibrin gels are both capable of iPSC maintenance in 3D

Recently, several studies have sought to identify materials capable of supporting iPSC for expansion and tissue engineering. Fibrin(ogen) has been found to be capable of this maintenance (34, 35). Because our group is interested in 3D stem cell differentiations with multiple stem cell types, we sought to corroborate these findings and determine if gel structure influences 3D iPSC culture. We encapsulated iPSC in PS (coarse) and HS (fine) gels and assessed pluripotent gene expression and qualitative cell morphology. Previous groups have shown that encapsulated iPSC must be allowed to proliferate for at least three days after seeding to lead to successful differentiations, so we assessed pluripotent gene expression after 1 and 3 days (35). After culturing iPSC within the two gel formulations and on Matrigel® (2D culture), we observed no difference in pluripotent gene expression (POU5F1 and NANOG) 1 and 3 days after passage among any of the culture groups (Figs 6E and 6F). Interestingly, iPSC in the fine HS gels formed compact, spheroid-like colonies, while iPSC in the looser PS gels appeared to remain mostly singularized, though this finding was purely qualitative and was not measured (Fig 6).

4. Conclusions

In the field of tissue engineering, there is a need for simple scaffolds that support angiogenesis, cell proliferation and remodeling, and exhibit tunable degradation rates. Fibrin gels are particularly promising because of their bioactivity; fibrin modulates the healing response *in situ* during wound healing. However, the rapid degradation rate of fibrin has limited its usefulness in 3D cell culture and tissue engineering. In this work, we demonstrated

that the fiber architecture and degradation rate of PEGylated fibrin can be tuned simply by changing the NaCl concentration in the fibrinogen solvent. Using our simple four-step fabrication method, increasing the NaCl concentration in the fibrinogen solvent from 145mM to 565mM results in HS PEG-fibrin gels with a final NaCl concentration 250mM. These HS gels exhibit fine fiber morphology, rendering them transparent compared to the opaque, coarse-fiber PS gels. The increased transparency of HS gels could be useful for 3D imaging experiments, but perhaps even more useful is our finding that HS gels degrade approximately three times more slowly than PS gels without affecting seeded cell viability, capillary-like network formation, or maintenance of iPSC. Furthermore, HS fibrin gels are stable *in vivo* and maintain the viability of delivered cells better than PS gels. Our previous work demonstrated that PEGylation of the fibrinogen also lowers the degradation rate of fibrin hydrogels, and for this reason we used only PEGylated fibrin gels. Howeer, we expect that even without PEGylation, HS fibrin gels would exhibit superior transparency and degradation kinetics versus PS gels. To our knowledge, this work represents the simplest reported method for controlling the transparency and degradation rate of fibrin without the need for fibrinolysis inhibitors. In our future studies, we will differentiate AFC and iPSC within the stable HS fibrin to create useful tissues for therapeutic implant, disease modeling, and drug screening. Specifically, we are interested in differentiating cardiac tissues and assessing this stable fibrin formulation in the repair of structural heart defects. Other future work should investigate the utility of this stable, transparent fibrin in other clinical and tissue engineering applications including wound healing (perhaps using a murine diabetic wound model), surgical glues (perhaps using AFM adhesion testing), cell delivery, developmental studies, and 3D cell culture and imaging.

5. Conflict of Interests

The authors declare no conflicts of interest.

6. Acknowledgements

This work was supported by the National Science Foundation grant number DGE-1553798 (awarded to DKJ and MLL), the National Institute of Health grant numbers 5T32HL072738-16 (awarded to EJV) and HL130436 (awarded to JGJ), and the American Heart Association grant number 19POST34380541 (awarded to MCV),

The authors would like to acknowledge Dr. Eric Wartchow and the Colorado Children's Hospital Microscopy Core for assistance with SEM imaging, the University of Colorado Flow Cytometry Core for assistance with amniotic

fluid cell FACS, Emily C. Beck, PhD, for her scientific expertise, Duncan Davis-Hall and the Chelsea Magin laboratory for assistance with bulk rheometry, and the University of Colorado Animal Care Facilities for assistance in animal handling training and care.

7. Author Contributions

Dillon Jarrell: Conceptualization, methodology, investigation, writing-original draft. Ethan Vanderslice: Conceptualizatoi, investigation, editing. Mallory Lennon: Formal analysis, editing. Anne Lyons: Investigation. Mitchell VeDepo: Visualization, editing. Jeffrey Jacot: Funding acquisition, supervision.

8. Data Availability

The raw data required to reproduce these findings are available to download from [INSERT PERMANENT WEB LINK(s)]. The processed data required to reproduce these findings are available to download from [INSERT PERMANENT WEB LINK(s)].

9. References

1. Khademhosseini A, Langer R. A decade of progress in tissue engineering. Nat Protoc. 2016;11(10):1775-81.
2. Kolesky DB, Homan KA, Skylar-Scott MA, Lewis JA. Three-dimensional bioprinting of thick vascularized tissues. Proc Natl Acad Sci U S A. 2016;113(12):3179-84.
3. Sarig U, Nguyen EB, Wang Y, Ting S, Bronshtein T, Sarig H, et al. Pushing the envelope in tissue engineering: ex vivo production of thick vascularized cardiac extracellular matrix constructs. Tissue Eng Part A. 2015;21(9-10):1507-19.
4. Williams DF. Challenges With the Development of Biomaterials for Sustainable Tissue Engineering. Front Bioeng Biotechnol. 2019;7:127.
5. Sengupta D, Waldman SD, Li S. From in vitro to in situ tissue engineering. Ann Biomed Eng. 2014;42(7):1537-45.
6. El-Sherbiny IM, Yacoub MH. Hydrogel scaffolds for tissue engineering: Progress and challenges. Glob Cardiol Sci Pract. 2013;2013(3):316-42.
7. Howard D, Buttery LD, Shakesheff KM, Roberts SJ. Tissue engineering: strategies, stem cells and scaffolds. J Anat. 2008;213(1):66-72.
8. Standeven KF, Ariens RA, Grant PJ. The molecular physiology and pathology of fibrin structure/function. Blood Rev. 2005;19(5):275-88.
9. Weisel JW. Fibrinogen and fibrin. Adv Protein Chem. 2005;70:247-99.
10. Chung E, Rytlewski JA, Merchant AG, Dhada KS, Lewis EW, Suggs LJ. Fibrin-based 3D matrices induce angiogenic behavior of adipose-derived stem cells. Acta Biomater. 2015;17:78-88.
11. Martino MM, Briquez PS, Ranga A, Lutolf MP, Hubbell JA. Heparin-binding domain of fibrin(ogen) binds growth factors and promotes tissue repair when incorporated within a synthetic matrix. Proc Natl Acad Sci U S A. 2013;110(12):4563-8.
12. Ahmann KA, Weinbaum JS, Johnson SL, Tranquillo RT. Fibrin degradation enhances vascular smooth muscle cell proliferation and matrix deposition in fibrin-based tissue constructs fabricated in vitro. Tissue Eng Part A. 2010;16(10):3261-70.
13. Benavides OM, Brooks AR, Cho SK, Petsche Connell J, Ruano R, Jacot JG. In situ vascularization of injectable fibrin/poly(ethylene glycol) hydrogels by human amniotic fluid-derived stem cells. J Biomed Mater Res A. 2015;103(8):2645-53.

14. Benavides OM, Quinn JP, Pok S, Petsche Connell J, Ruano R, Jacot JG. Capillary-like network formation by human amniotic fluid-derived stem cells within fibrin/poly(ethylene glycol) hydrogels. Tissue Eng Part A. 2015;21(7-8):1185-94.
15. Collet JP, Park D, Lesty C, Soria J, Soria C, Montalescot G, et al. Influence of fibrin network conformation and fibrin fiber diameter on fibrinolysis speed: dynamic and structural approaches by confocal microscopy. Arterioscler Thromb Vasc Biol. 2000;20(5):1354-61.
16. Kjaergard HK, Weis-Fogh US. Important factors influencing the strength of autologous fibrin glue; the fibrin concentration and reaction time--comparison of strength with commercial fibrin glue. Eur Surg Res. 1994;26(5):273-6.
17. Laurens N, Koolwijk P, de Maat MP. Fibrin structure and wound healing. J Thromb Haemost. 2006;4(5):932-9.
18. Nair CH, Shah GA, Dhall DP. Effect of temperature, pH and ionic strength and composition on fibrin network structure and its development. Thromb Res. 1986;42(6):809-16.
19. Sidelmann JJ, Gram J, Jespersen J, Kluft C. Fibrin clot formation and lysis: basic mechanisms. Semin Thromb Hemost. 2000;26(6):605-18.
20. Kurniawan NA, van Kempen THS, Sonneveld S, Rosalina TT, Vos BE, Jansen KA, et al. Buffers Strongly Modulate Fibrin Self-Assembly into Fibrous Networks. Langmuir. 2017;33(25):6342-52.
21. Li W, Sigley J, Pieters M, Helms CC, Nagaswami C, Weisel JW, et al. Fibrin Fiber Stiffness Is Strongly Affected by Fiber Diameter, but Not by Fibrinogen Glycation. Biophys J. 2016;110(6):1400-10.
22. Ferry JD, Morrison PR. Preparation and properties of serum and plasma proteins; the conversion of human fibrinogen to fibrin under various conditions. J Am Chem Soc. 1947;69(2):388-400.
23. Muller MF, Ris H, Ferry JD. Electron microscopy of fine fibrin clots and fine and coarse fibrin films. Observations of fibers in cross-section and in deformed states. J Mol Biol. 1984;174(2):369-84.
24. Eyrich D, Brandl F, Appel B, Wiese H, Maier G, Wenzel M, et al. Long-term stable fibrin gels for cartilage engineering. Biomaterials. 2007;28(1):55-65.
25. Davis HE, Miller SL, Case EM, Leach JK. Supplementation of fibrin gels with sodium chloride enhances physical properties and ensuing osteogenic response. Acta Biomater. 2011;7(2):691-9.
26. Di Stasio E, Nagaswami C, Weisel JW, Di Cera E. Cl- regulates the structure of the fibrin clot. Biophys J. 1998;75(4):1973-9.
27. Kostelansky MS, Lounes KC, Ping LF, Dickerson SK, Gorkun OV, Lord ST. Calcium-binding site beta 2, adjacent to the "b" polymerization site, modulates lateral aggregation of protofibrils during fibrin polymerization. Biochemistry. 2004;43(9):2475-83.
28. Sacchi V, Mittermayr R, Hartinger J, Martino MM, Lorentz KM, Wolbank S, et al. Long-lasting fibrin matrices ensure stable and functional angiogenesis by highly tunable, sustained delivery of recombinant VEGF164. Proc Natl Acad Sci U S A. 2014;111(19):6952-7.
29. Robinson M, Douglas S, Michelle Willerth S. Mechanically stable fibrin scaffolds promote viability and induce neurite outgrowth in neural aggregates derived from human induced pluripotent stem cells. Sci Rep. 2017;7(1):6250.
30. Hotaling NA, Bharti K, Kriel H, Simon CG, Jr. DiameterJ: A validated open source nanofiber diameter measurement tool. Biomaterials. 2015;61:327-38.
31. Kogut I, McCarthy SM, Pavlova M, Astling DP, Chen X, Jakimenko A, et al. High-efficiency RNA-based reprogramming of human primary fibroblasts. Nat Commun. 2018;9(1):745.
32. Loukogeorgakis SP, De Coppi P. Concise Review: Amniotic Fluid Stem Cells: The Known, the Unknown, and Potential Regenerative Medicine Applications. Stem Cells. 2017;35(7):1663-73.
33. Petsche Connell J, Camci-Unal G, Khademhosseini A, Jacot JG. Amniotic fluid-derived stem cells for cardiovascular tissue engineering applications. Tissue Eng Part B Rev. 2013;19(4):368-79.
34. Gandhi JK, Knudsen T, Hill M, Roy B, Bachman L, Pfannkoch-Andrews C, et al. Human Fibrinogen for Maintenance and Differentiation of Induced Pluripotent Stem Cells in Two Dimensions and Three Dimensions. Stem Cells Transl Med. 2019;8(6):512-21.
35. Kerscher P, Turnbull IC, Hodge AJ, Kim J, Seliktar D, Easley CJ, et al. Direct hydrogel encapsulation of pluripotent stem cells enables ontomimetic differentiation and growth of engineered human heart tissues. Biomaterials. 2016;83:383-95.

Fig 1: Increasing salinity of fibrinogen solvent with NaCl impacts fibrin opacity. pH (A) and $CaCl_2$ concentration (B) of gel precursor solutions do not impact gel transparency or morphology. Increasing fibrinogen concentration decreases transparency (C). However, increasing NaCl concentration in fibrinogen solution prior to gelation increases final gel transparency (D, E). For reference, PBS absorbance of 352 nm light is 0.06.

Fig 2: Changing salinity of fibrinogen solution alters fibrin gel properties. SEM images of fiber morphology (A, B) reveal that increasing salt concentration decreases porosity and fiber size (C). Young's moduli of individual fibers measured by AFM (D), Young's and Storage Modulus of the bulk materials measured by parallel plate rheometry (E,F), Swelling Ratio (G), and growth factor sequestering (F) are also significantly affected by salinity during gelation.

Fig 3: Increased salinity does not affect viability of encapsulated cells or ability to form endothelial networks. LIVE/DEAD® analysis stains Live cells green and Dead cells red. No significant difference in viability detected between amniotic fluid cells seeded in HS and PS gels (A-F), as quantified in (I). Both HS and PS gels support capillary-like network formation when seeded with GFP-HUVEC (green) and HDF (stained red with anti-α-smooth muscle actin) (G, H). Scale bars 50um

Fig 4: Transparent high salt (HS) fibrin degrades slowly *in vitro*. Increasing salt concentration yields fibrin with decreasing degradation kinetics when treated with Papain (no cells, panel A) and when seeded with AFC (B). 1 mg/mL 6-aminocaproic acid (ACA) prevents cell-mediated fibrinolysis, but HS gels are stable without ACA for at least 14d. Images of AFC-seeded gels degrading over 14d shown in panels C-I. By day 14, PS gels are completely degraded while HS gels are stable and continue to support 3D AFC culture (G-I). Scale bars of 200x images = 50um.

Fig 5: HS gels are stable *in vivo* after 7d, but PS gels degraded completely. HS and PS precursor solutions were mixed with GFP-HUVEC (green) and HDF (stained with Vimentin, red) and injected subcutaneously into athymic mice (N). After 7d, HS gels remained intact (H&E, A and B) and delivered cells remained viable (IF, C-G). Remaining gel indicated with arrows. PS gels degraded completely; no gel or delivered cells were detectable after 7d (H-M). Scale bars 500um (A, H), 200um (B-M), 50um (G).

Fig 6: PS and HS gels support iPSC expansion and pluripotency. Both gel types maintain expression of pluripotency genes POU5F1 (E) and NANOG (F) compared to standard 2D Matrigel® culture. HS gels appear to drive formation of spheroid-like iPSC colonies (A,B) while PS gels appear to maintain singularized iPSC (C,D). Scale bars 50um.

Supplementary Fig 1: Expression profile of amniotic fluid cells closely resembles mesenchymal stem cells. Amniotic fluid cells (AFC) sorted using fluorescent-activated cell sorting were positive for MSC markers CD90, CD105, CD73, and CD117 (c-kit) and negative for CD34, C45, CD19, HLA-DR, and CD133. Red populations represent negative control unstained AFC, green populations represent stained AFC.

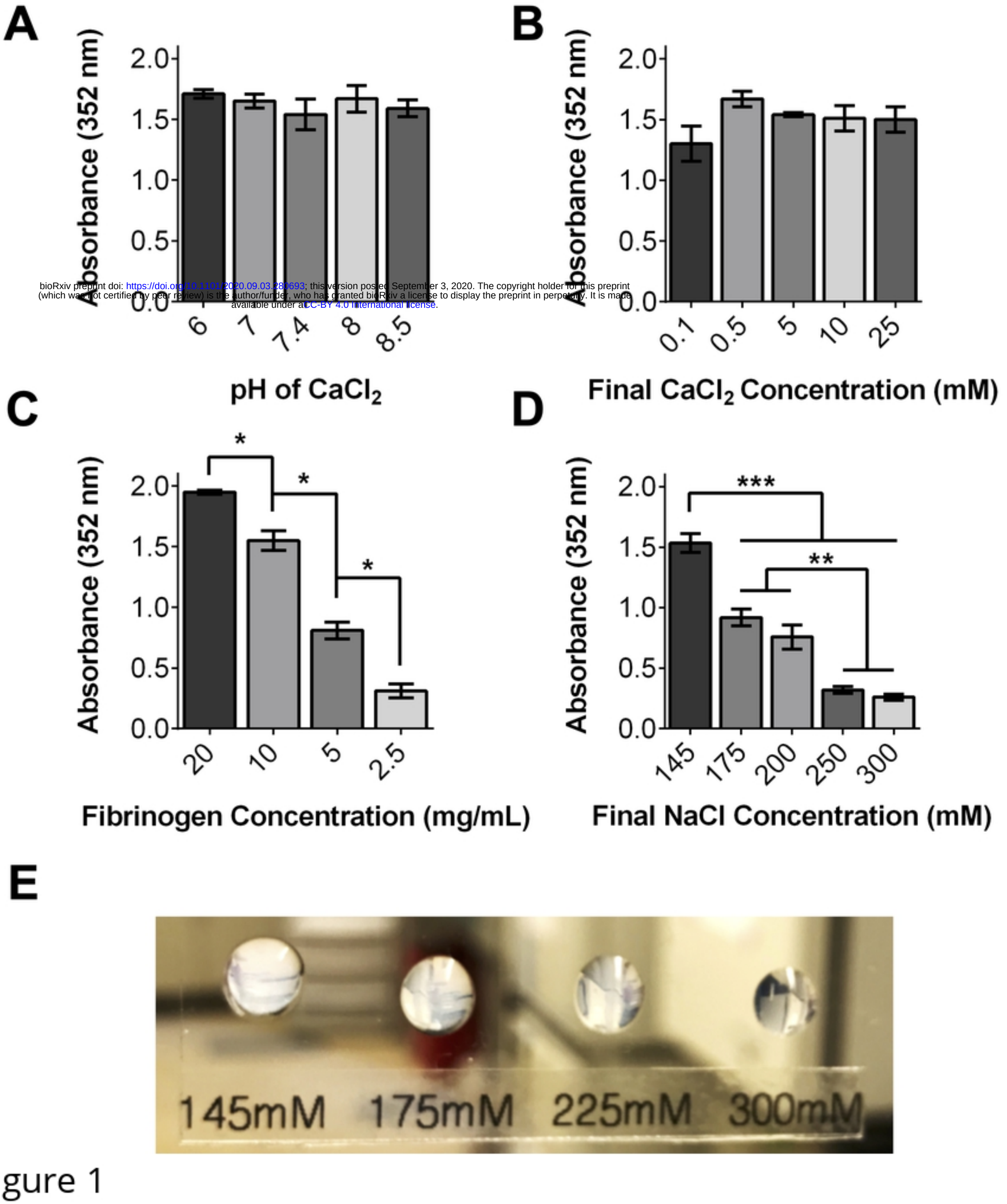

Figure 1

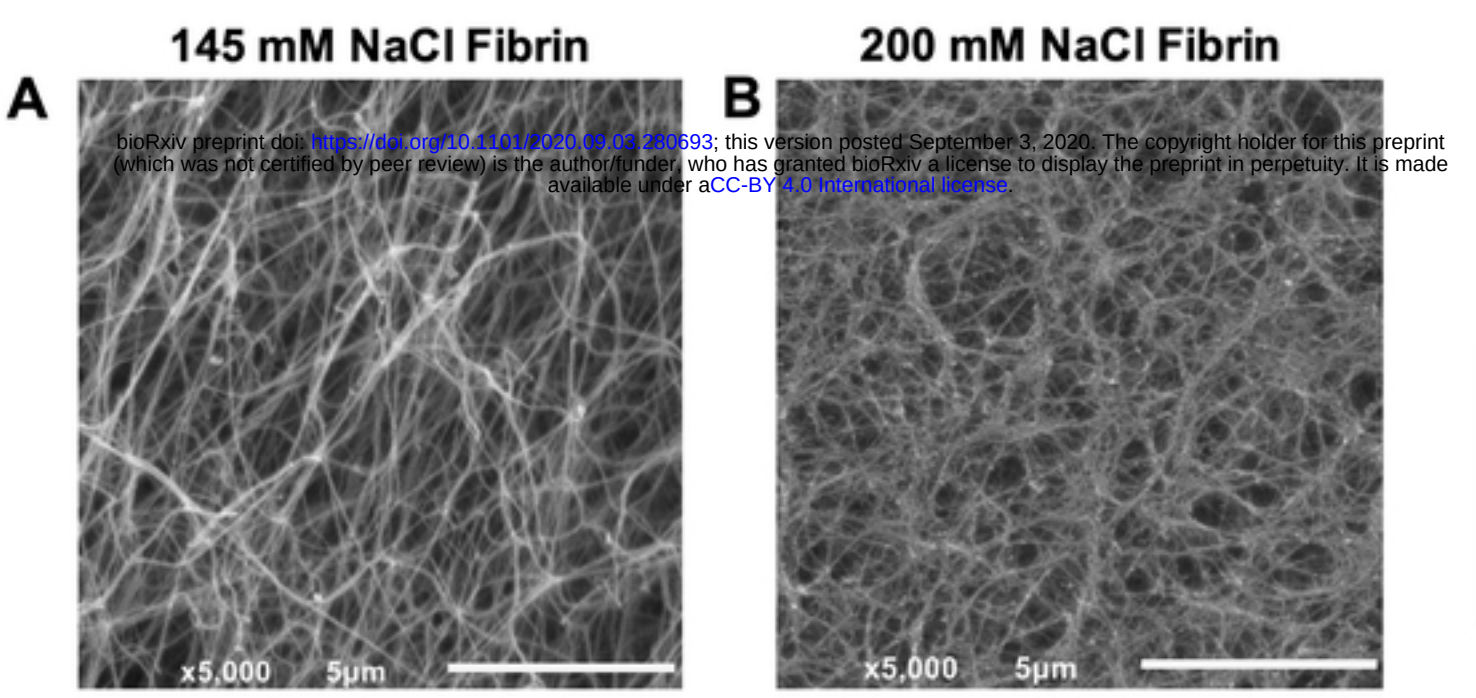

C

	Porosity (%)	Fiber Diameter (nm)
200 mM	48.8%	58 +/- 29
145 mM	54.50%	74 +/- 43

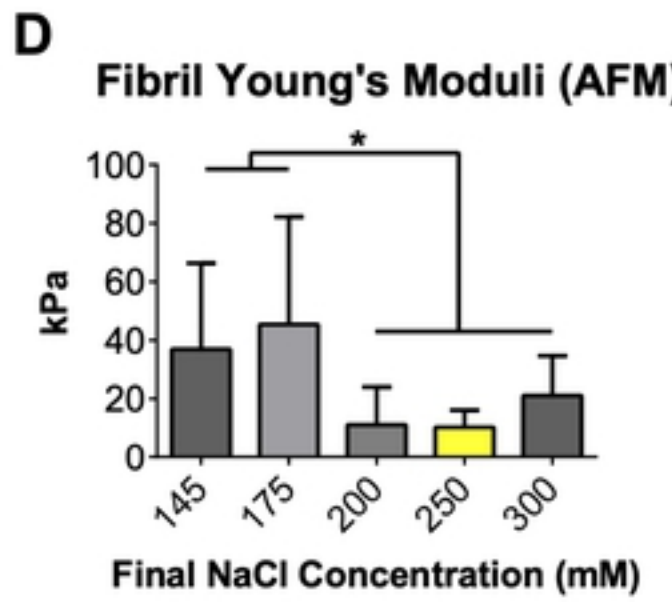

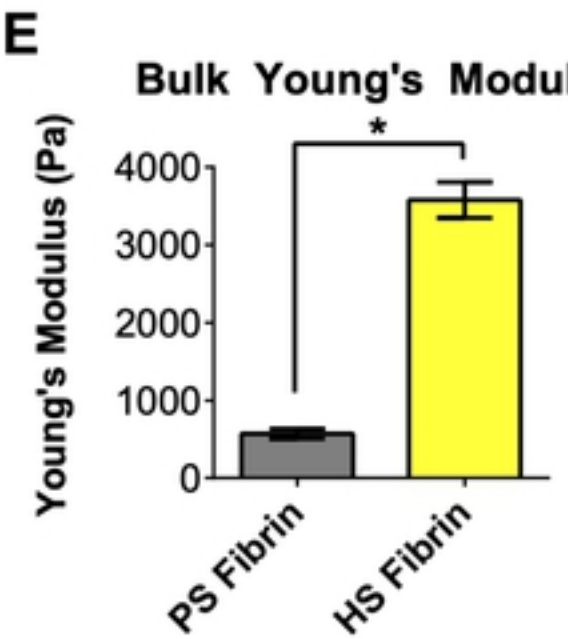

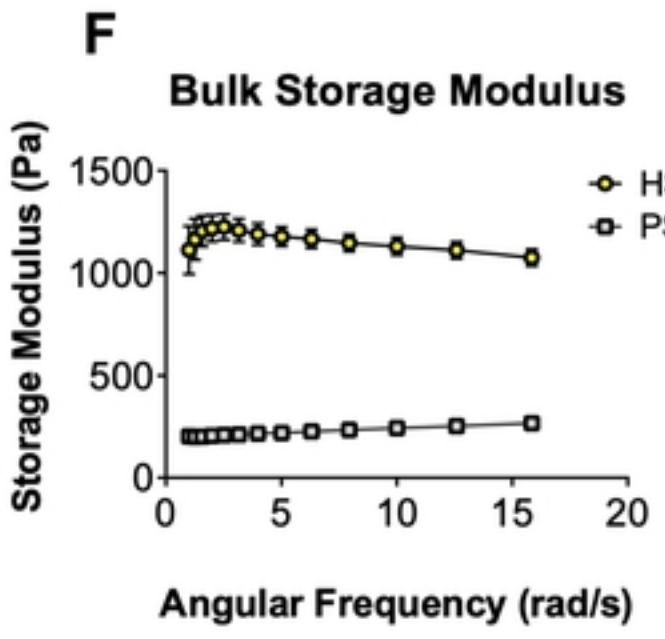

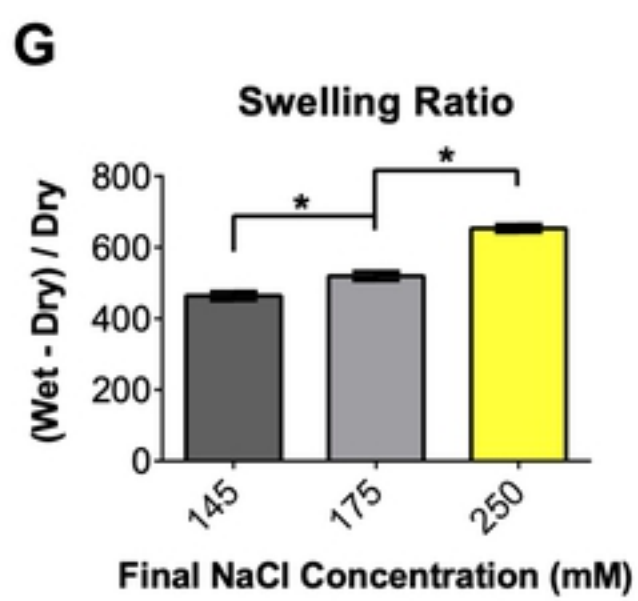

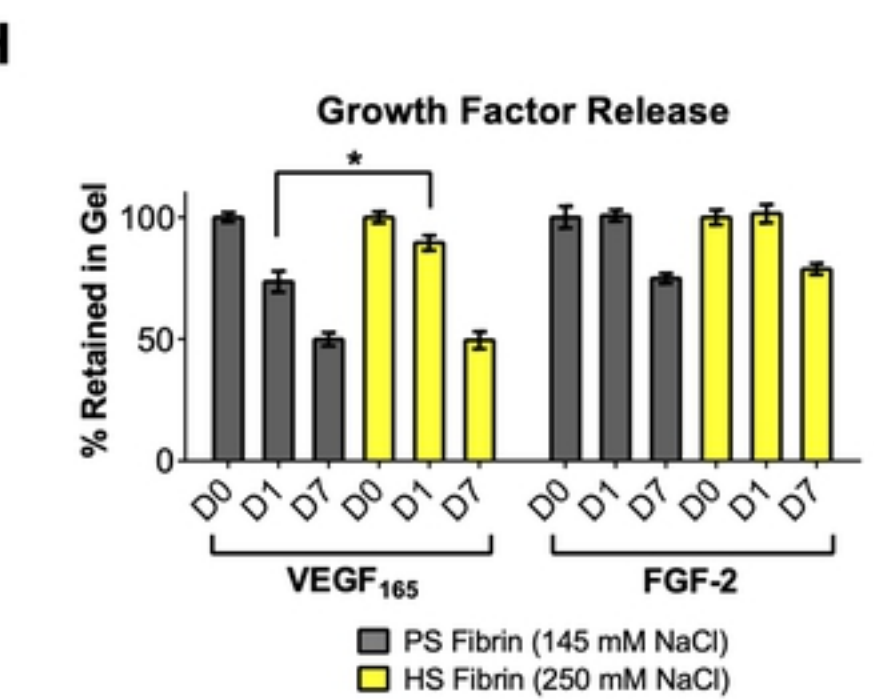

Figure 2

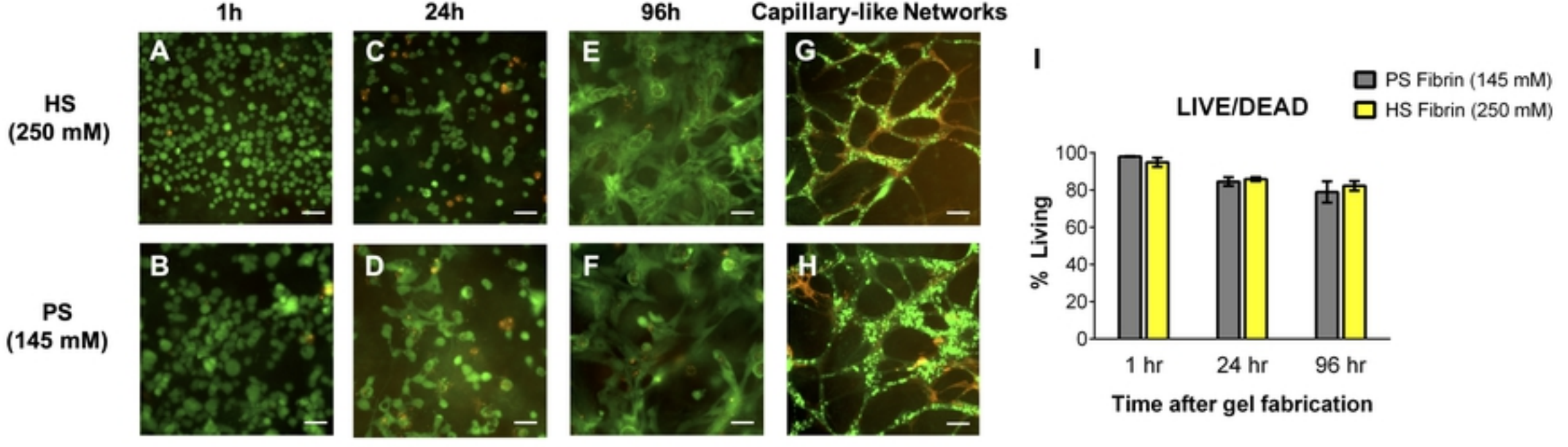
1h
24h
96h
Capillary-like Networks
HS
(250 mM)
PS
(145 mM)
A
B
C
D
E
F
G
H
I
LIVE/DEAD
PS Fibrin (145 mM)
HS Fibrin (250 mM)
% Living
100
80
60
40
20
0
1 hr
24 hr
96 hr
Time after gel fabrication

Figure 3

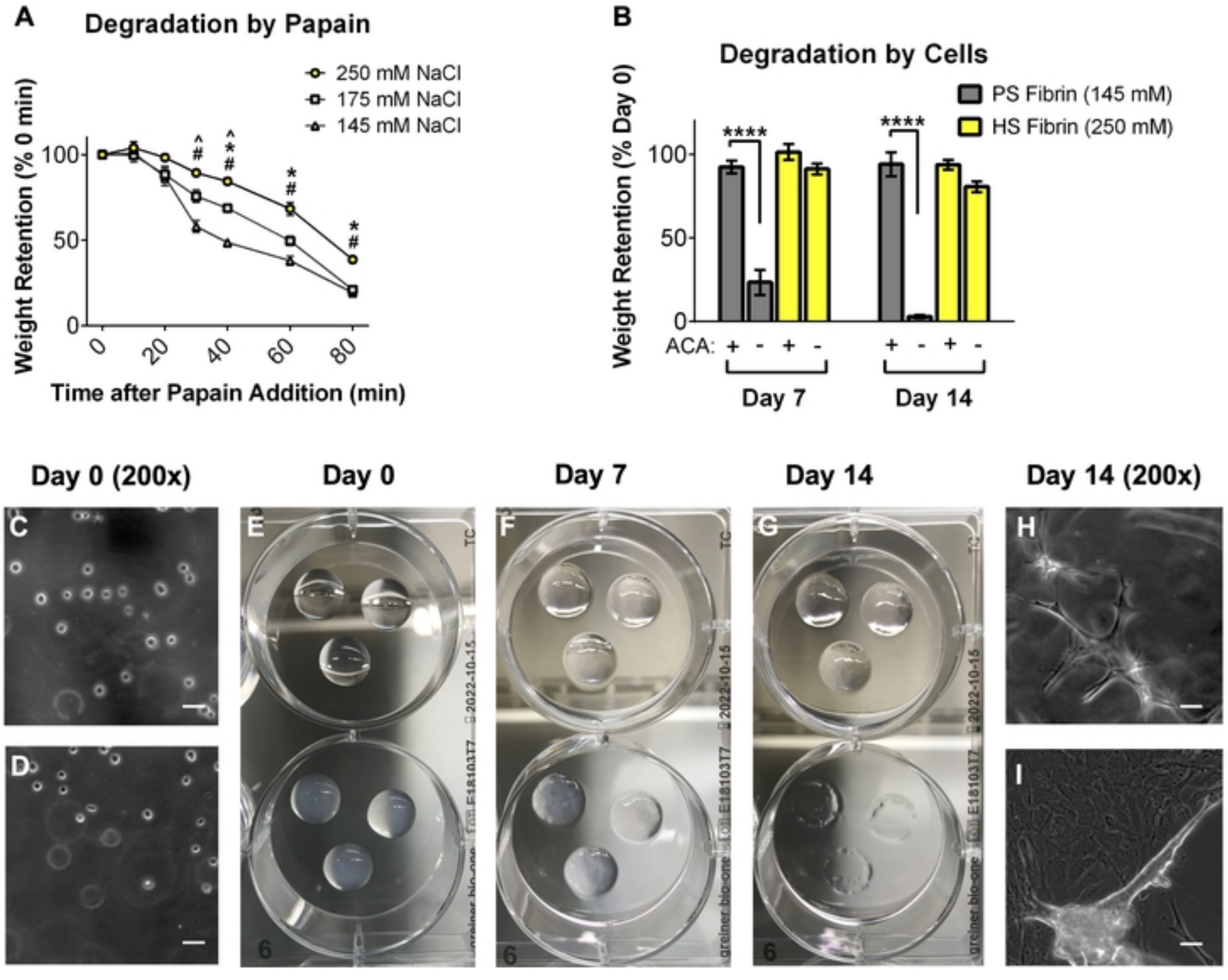
A
Degradation by Papain
250 mM NaCl
175 mM NaCl
145 mM NaCl
Weight Retention (% 0 min)
100
50
0
0
20
40
60
80
Time after Papain Addition (min)
B
Degradation by Cells
PS Fibrin (145 mM)
HS Fibrin (250 mM)
Weight Retention (% Day 0)
****
****
100
50
0
ACA: + - + -
+ - + -
Day 7
Day 14
Day 0 (200x)
Day 0
Day 7
Day 14
Day 14 (200x)
HS
(250 mM)
PS
(145 mM)
C
D
E
F
G
H
I

Figure 4

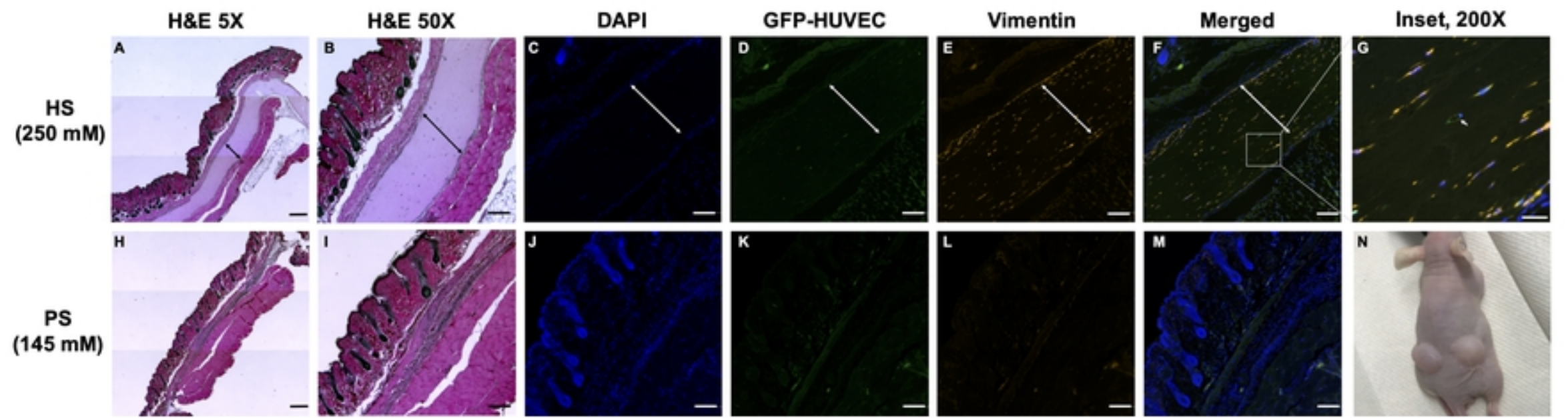
H&E 5X
H&E 50X
DAPI
GFP-HUVEC
Vimentin
Merged
Inset, 200X
HS
(250 mM)
PS
(145 mM)
A
B
C
D
E
F
G
H
I
J
K
L
M
N

Figure 5

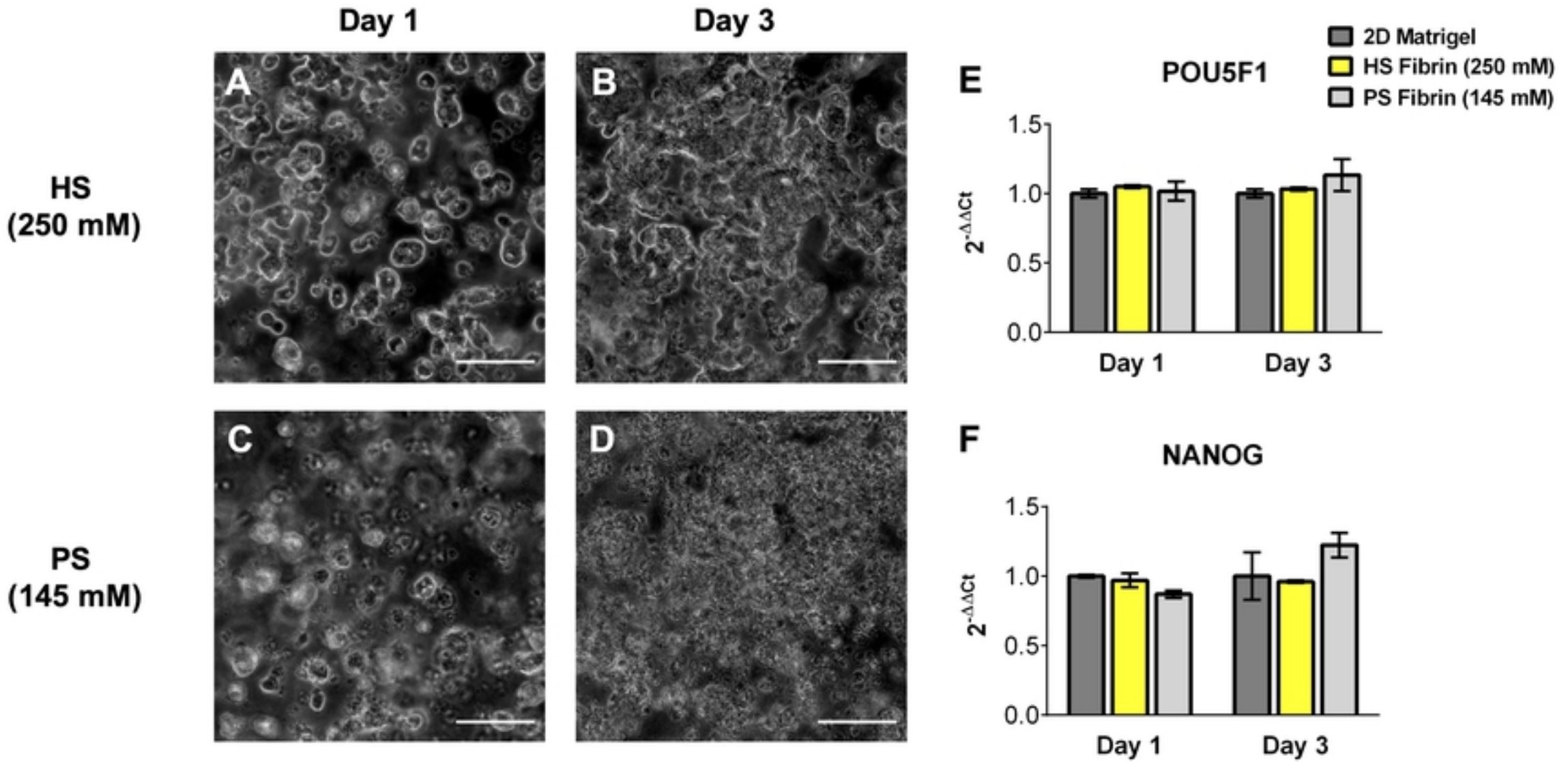
Day 1
Day 3
HS
(250 mM)
PS
(145 mM)
A
B
C
D
E
POU5F1
2D Matrigel
HS Fibrin (250 mM)
PS Fibrin (145 mM)
1.5
1.0
0.5
0.0
2-ΔΔCt
Day 1
Day 3
F
NANOG
1.5
1.0
0.5
0.0
2-ΔΔCt
Day 1
Day 3

Figure 6

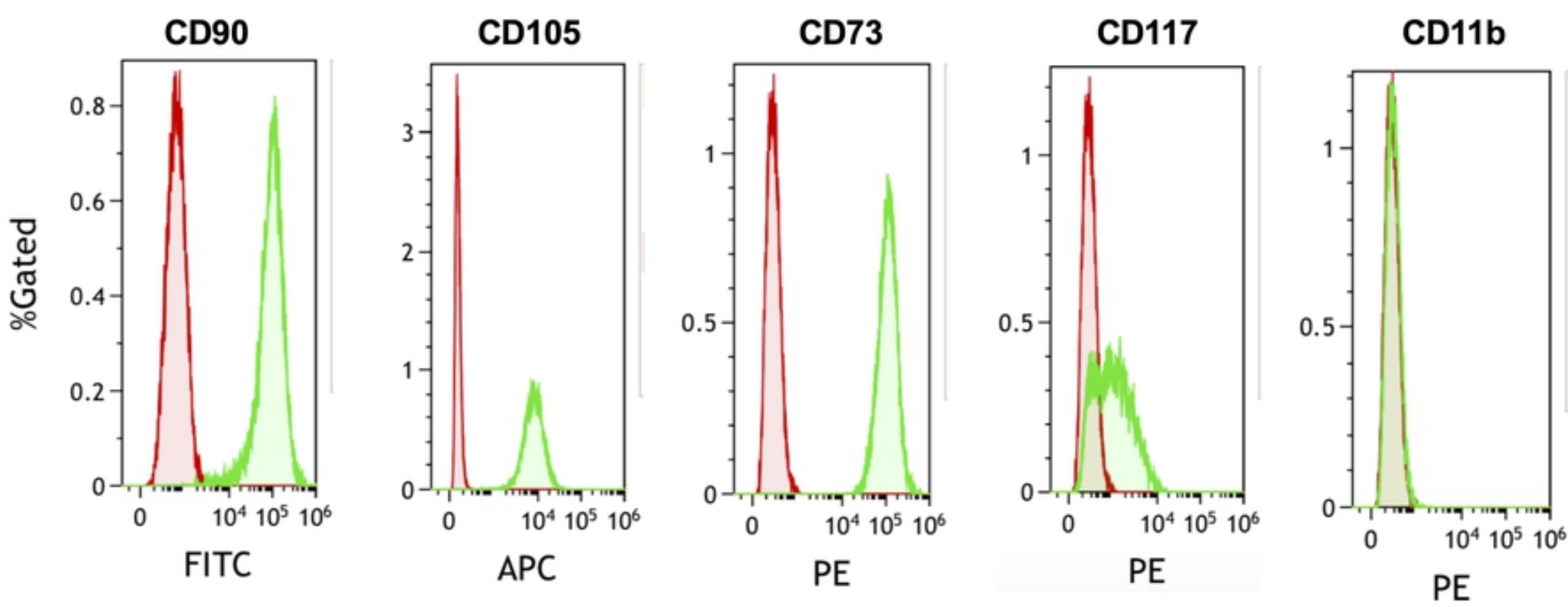

Supplementary Figure 1